Eur. Phys. J. A (2016) **52**: 66
DOI 10.1140/epja/i2016-16066-5

THE EUROPEAN PHYSICAL JOURNAL A

Regular Article – Theoretical Physics

# Neutron stars interiors: Theory and reality*

J.R. Stone[1,2,a]

[1] Department of Physics, University of Oxford, OX1 3PU Oxford, UK
[2] Department of Physics and Astronomy, University of Tennessee, Knoxville, TN 37996, USA

Received: 21 August 2015 / Revised: 25 January 2016
Published online: 24 March 2016 – 
Communicated by D. Blaschke

**Abstract.** There are many fascinating processes in the universe which we observe in more detail thanks to increasingly sophisticated technology. One of the most interesting phenomena is the life cycle of stars, their birth, evolution and death. If the stars are massive enough, they end their lives in a core-collapse supernova explosion, one of the most violent events in the universe. As a result, the densest objects in the universe, neutron stars and/or black holes, are created. The physical basis of these events should be understood in line with observation. Unfortunately, available data do not provide adequate constraints for many theoretical models of dense matter. One of the most open areas of research is the composition of matter in the cores of neutron stars. Unambiguous fingerprints for the appearance and evolution of particular components, such as strange baryons and mesons, with increasing density, have not been identified. In particular, the hadron-quark phase transition remains a subject of intensive research. In this contribution we briefly survey the most promising observational and theoretical directions leading to progress in understanding high density matter in neutron stars. A possible way forward in modeling high-density matter is outlined, exemplified by the quark-meson-coupling model (QMC). This model makes connection between hadronic structure and the underlying quark make-up. It offers a natural explanation for the saturation of nuclear force and treats high-density matter, containing the full baryon octet, in terms of four uniquely defined parameters adjusted to properties of symmetric nuclear matter at saturation.

## 1 Introduction

The structure of matter at high density and temperature is one of the central questions of current theoretical physics. Answering this question requires the joint efforts of nuclear, particle and astrophysics theorists, combined with tests based on the most advanced astrophysical observation data and relevant terrestrial experiments.

In the generally accepted Quantum Chromodynamics (QCD) phase diagram, expressed in terms of temperature and baryon number density (see fig. 1), two extreme regions can be identified. The best realization of nuclear matter at low (zero) temperature and high baryon number density (several times higher that the saturation density of symmetric nuclear matter) is found in the cores of cold neutron stars and, at somewhat higher temperature, in core-collapse supernovae (CCS). The other extreme is at low (zero) baryon number density and extremely high temperature (several hundred MeV). This region of the phase diagram corresponds to conditions in the early universe. The adjacent region with lower temperatures and somewhat higher baryonic densities can, in principle, be probed in existing terrestrial heavy ion collisions, at LHC, RHIC and GSI. Extension towards even higher chemical potentials and lower temperatures is expected at planned facilities, FAIR at GSI and NICA in Dubna. One of the key questions is the location of the critical point where the hadronic and quark-gluon phases coexist. There is an extensive beam scan campaign at RHIC, performed by the STAR Collaboration, in this direction, but no final conclusion has yet been reached. The position of the critical point has important implications for the location of the hadronic-quark phase transition in neutron stars and CCS [1].

In this paper we address the fundamental question as to whether we have enough experimental and observational data to compare with a current theory to give answers to questions concerning properties of high-density matter in the low temperature and high baryonic density region of the QCD diagram. In sect. 2 we introduce the definition of the Equation of State (EoS) and its connection with nuclear and particle models. Section 3 is devoted to the up-to-date constraints on the EoS from observation

* Contribution to the Topical Issue on "Exotic matter in neutron stars" edited by David Blaschke, Jürgen Schaffner-Bielich, Hans-Josef Schulze.

[a] e-mail: j.stone@physics.ox.ac.uk

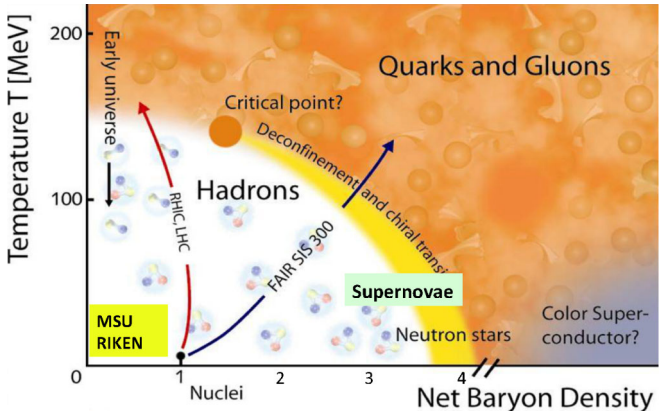


**Fig. 1.** The QCD phase diagram, adopted from `www.gsi.de`, showing the temperature and baryon density ranges for different phases of hadronic and quark matter.

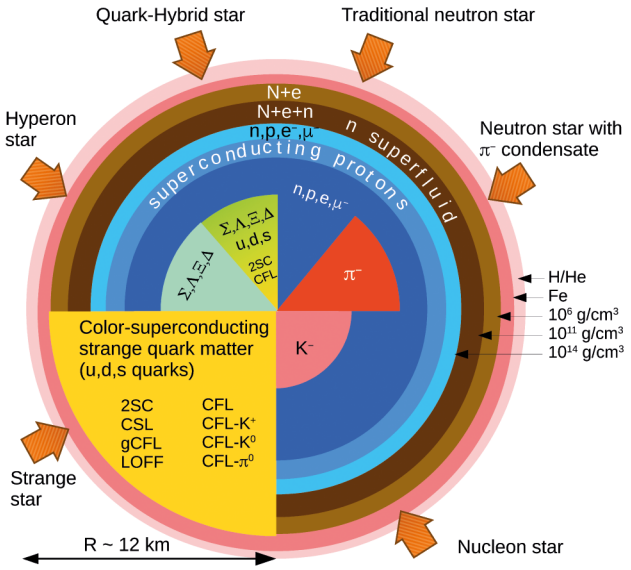


**Fig. 2.** Proposed structure of a cold neutron star. Redrawn from ref. [2].

of neutron stars and CCS. Constraints coming from terrestrial experiments with heavy-ion collisions and hypernuclei, as well as, potentially, from lattice QCD, are briefly discussed in sect. 4, followed by discussion of the Quark-Meson-Coupling (QMC) model, which offers a new perspective in description of low energy nuclear and particle phenomena in sect 5. Summary and conclusions are presented in sect. 6.

## 2 Equation of State of high-density matter

The key property of high-density matter is the Equation of State (EoS) from which the relation between the pressure $P$, energy density $\epsilon$, and temperature $T$, of the matter, can be derived. We have

$$P = \rho^2 \left( \frac{\partial(\epsilon/\rho)}{\partial \rho} \right)_{s/\rho} \qquad \epsilon(\rho, T) = \sum_i \epsilon_i(\rho, T), \qquad (1)$$

where $\rho$ is particle number density, $\epsilon$ is the energy density and the summation carries over all $i$ constituents present in the matter. The two key points here are: i) the EoS critically depends on the constituents of the matter and the interactions between them and ii) $\epsilon(\rho, T)$ is unknown and can only be determined from nuclear and/or particle physics models. Limitations of these models are the main source of ambiguity in theoretical determination of the EoS of high-density matter occurring in astronomical objects and terrestrial systems. There are many variants of microscopic and phenomenological models of hadronic matter with different levels of complexity. To name a few, mean-field non-relativistic and relativistic models, *ab initio* models with two- and three-body nucleon-nucleon (N-N) interactions and chiral effective field theory are frequently used. There is also a wide choice of components of hadronic matter, from nucleons only to matter including the full baryon octet and baryon resonances (p, n, $\Lambda$, $\Sigma$, $\Xi$, $\Delta$), and mesons ($\pi$, $K$, H-dibaryon condensates).

QCD predicts matter in the form of a quark liquid in a colour superconducting state at high density and low temperature [2–4]. Unfortunately theoretical understanding of the appearance and properties of quark matter in the interior of neutron stars is very uncertain because of limited knowledge of the strong interaction in medium. Many models based on different techniques are in use, including, for example, different forms of the MIT bag [5–7], Nambu–Jona-Lasinio [8, 9], Chromo-Dielectric [10, 11], Dyson-Schwinger [12, 13] and perturbative approaches to QCD [14–16].

The extreme conditions in neutron stars allow their theoretical description as hybrid stars (see fig. 2), composed of a nucleon-only crust with a core of strange baryons and mesons with stable quark matter in the center, or as strange stars, made of absolutely stable strange quark matter (a configuration of matter more stable than the most stable atomic nucleus, $^{62}$Ni), possibly with a thin nuclear crust of density below the neutron drip threshold. Other theories would include hyperonic stars. Models of neutron superfluidity and proton superconductivity and different phases of colour super-conductive quark matter (yellow segments) are also included in the picture.

Attempts to distinguish between these different options leave the choice unresolved. The lack of knowledge of the forces acting between the elementary particles leads to models with a large number of parameters, too many to be determined unambiguously from experiments and observations. For example, Dutra *et al.* [17] collected 240 non-relativistic mean-field models based on the Skyrme interaction, the effective density-dependent force, determined by the aid of 10–15 adjustable parameters. They assessed the ability of each parameterization to satisfy a series of constraints derived from macroscopic properties of nuclear matter in the vicinity of nuclear saturation density at zero temperature obtained by the liquid-drop model, and their density dependence extracted from experiments with giant resonances and heavy-ion collisions. Out of the 240

models, only sixteen were shown to satisfy all constraints. Additional, more microscopic, constraints on the density dependence of the neutron and proton effective mass in $\beta$-equilibrium matter, Landau parameters of symmetric and pure neutron matter, and observational data on high- and low-mass cold neutron stars further reduced this number to five, a very small group of recommended Skyrme parameterizations to be used in future applications of the Skyrme interaction of nuclear-matter–related observables. Disappointingly, the five successful parameter sets show no common features, being arrived at by fitting different observational and experimental properties.

Recently, a set of 263 relativistic mean-field models, including those frequently used in the literature, was examined in a similar fashion [18]. The analysis has shown that very few models satisfy the most up-to-date constraints.

Mean field models discussed above are usually constructed with the constraint that basic properties of symmetric nuclear matter (equal number of protons and neutrons, no Coulomb interaction), namely saturation energy $E_0 \sim -16\,\mathrm{MeV}$ at density $\rho_0 \sim 0.16\,\mathrm{fm}^{-3}$, be predicted correctly. This requirement is not imposed on so-called "realistic" models, which start from a bare two-body (N-N) interaction and include the effect of the medium using techniques such as Bruckner-Hartree-Fock or its relativistic counterpart Dirac-Bruckner-Hartree-Fock. The basic saturation properties fail to be reproduced satisfactorily [19, 20] unless three-body forces are added. These forces are also needed in other scenarios, such as variational methods [21] and Chiral Effective Field Theory [22]. This addition increases uncertainty in the models, as three-body forces are not well known and contain additional variable parameters.

Considerable uncertainty exists in the calculation of binding energy per particle in an even simpler system, pure neutron matter at sub-saturation density. Pure neutron matter does not exist in nature and the only theoretical constraint is that it should not have a bound state. The modern chiral effective field approach in next-to-next-to-next-to-leading order (N3LO) yields an EoS with the uncertainty depicted by the red (shaded) area in fig. 9 of ref. [22], overlying many other EoS of pure neutron matter obtained in other models.

The coexistence of hadronic and quark phases in the neutron star interior and the transition between them is usually considered in one of two ways. In the first the hadronic matter is made only of nucleons (N), whilst in the second it contains heavy strange baryons (Y) and boson condensates. The composition of the hadronic phase affects significantly the EoS at supra-saturation density and is related directly to the maximum mass of a neutron star. To comply with observation, the EoS of a hybrid star has to be stiff enough to produce a neutron star with gravitational mass around 2 $M_\odot$. This constraint is not difficult to satisfy with EoS of high-density matter containing only nucleons. However, any additional degree of freedom of the matter related to non-nucleonic components softens the EoS making production of a heavy neutron star more difficult. Keeping in mind that the EoS depends not only on composition, but also on interactions between all the constituents, it is vital to improve our knowledge of N-Y and Y-Y interactions. Furthermore, we have to learn more of the hadron-quark phase transition. Does it happen at densities lower than the threshold density for appearance of hyperons, hence suppressing them completely? Does the neutron star interior go through the hyperonic (and boson condensate) phases before it reaches the quark phase? Or, finally, does it never happen since the transition to quark matter occurs only at densities higher then those than can be achieved in the cores of neutron stars? There is an extensive literature on this subject, which is beyond the scope of this paper, however no convincing answer has emerged.

A way forward may be the study by Alford *et al.* [23] who suggested generic conditions for stable hybrid stars. The mass-radius curve of hybrid stars was studied, assuming a single first-order phase transition between nuclear and quark matter, with a sharp interface between the quark matter core and nuclear matter mantle. A generic parametrization of the quark matter EoS with a constant, *i.e.* density-independent, speed of sound was used. The authors suggested that this parametrization provides a framework for comparison and empirical testing of models of quark matter. It is interesting to note that the latest continuous QCD calculations suggest a sharp transition between the hadronic and quark phase [25].

There has been an interesting recent development in research on hybrid stars [26], in which a relativistic mean-field EoS with density-dependent couplings with the nucleons treated in the quasi-particle framework, was chosen for the hadronic phase and the higher-order repulsive interactions were included in the NJL model based EoS of the quark phase. This model led to a strong first-order phase transition with large latent heat (reflecting the energy-density jump at the phase transition), which fulfils the criterion for a transition to otherwise disconnected third-family branch of compact stars in the mass-radius relationship [27]. These "twin" stars in the third branch are predicted to have high maximum mass ($\sim 2\ M_\odot$) very similar to stars in the second (regular) second branch.

The lack of adequate constraints on the theoretical predictions of the EoS has led to efforts to construct a hybrid empirical EoS, made up of components from theory, astrophysical observation and terrestrial data. We will discuss these components more fully in sect. 3. Here we mention one such example presented by Steiner *et al.* [28] and shown in fig. 3. The authors used their analysis of recent observations of both transiently accreting and bursting X-ray sources and determined the 68% and 95% confidence intervals of the EOS of dense matter, with the estimated uncertainty of the pressure approximately 30%–50% at all densities achievable in neutron star interiors. These data have been combined with contributions coming from analysis of heavy-ion collision experiments and Quantum Monte Carlo models at low densities and pressures to provide an EoS applicable over a wide range. Such an approach may have some practical value but is limited since, at any number density, the predicted pressure range is wide.

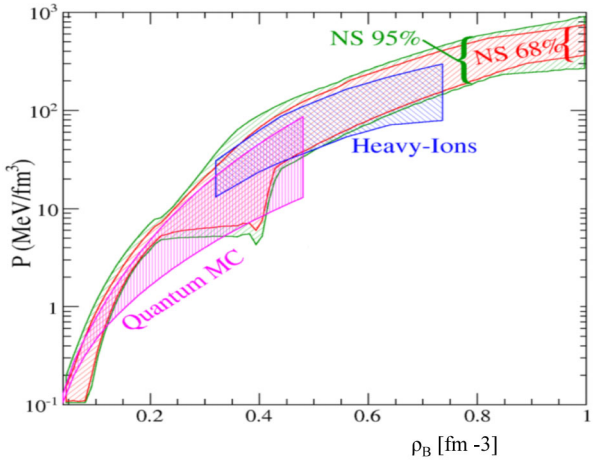


**Fig. 3.** Pressure as predicted from astrophysical observations in combination with Quantum Monte Carlo calculation and constraints obtained from analysis of heavy-ion collision experiments. For more explanation see text. Adopted from ref. [28].

## 3 Observational constraints on high-density EoS

### 3.1 Gravitational mass of cold neutron stars

The gravitational mass and radius of a cold non-rotating neutron star can be obtained from the Tolman-Oppenheimer-Volkoff (TOV) equations for hydrostatic equilibrium of a spherical object with isotropic density distribution in general relativity:

$$\frac{\mathrm{d}P(r)}{\mathrm{d}r} = -\frac{GM(r)\epsilon(r)}{r^2} \times \frac{(1+P(r)/\epsilon(r)c^2)(1+4\pi r^3 P(r)/M(r)c^2)}{1-2GM(r)/rc^2} \quad (2)$$

$$M(r) = \int_0^r 4\pi r'^2 \epsilon(r')\mathrm{d}r'. \quad (3)$$

Solution of these coupled equations yields sequences of neutron star models with a range of values for the central energy density $\epsilon(0)$ (note that here we use energy density $\epsilon$) instead of free energy density $f$ as we deal with cold neutron stars). Integration of eqs. (2) and (3) for any specified $\epsilon(0)$, gives directly the corresponding values for the total gravitational mass $M(R)$ and radius $R$ of the star (the surface being at the location where the pressure reaches zero).

Two features are important here. First, the dependence of pressure $P(r)$ on energy density $\epsilon(r)$ —the EoS —is required input to the TOV equations, bringing in the microphysics. Second, the output only yields gravitational mass $M(R)$ as a function of a corresponding radius $R$. This is a major source of difficulty in relating observation to theory because data on mass and radius on the same star is very hard to obtain with high enough accuracy. It follows that even very accurate determination of neutron star mass, currently available and summarized in table 1, is a necessary but not a sufficient constraint for selection of a realistic EoS. The situation is illustrated in fig. 4. The largest observed neutron star masses serve to eliminate some EoS, but others satisfy this requirement and it is not possible to choose between them.

**Table 1.** Examples of the most accurately measured neutron star masses.

| Pulsar | $M/M_\odot$ | Error | Reference |
|---|---|---|---|
| PSR J0737-3039 | 1.249 | 0.001 | [29] |
| PSR B1913+16 | 1.4414 | 0.0002 | [30] |
| PSR J1903+0327 | 1.667 | 0.021 | [31] |
| PSR J1614-2230 | 1.97 | 0.04 | [32] |
| PSR J0348+0432 | 2.01 | 0.04 | [33] |

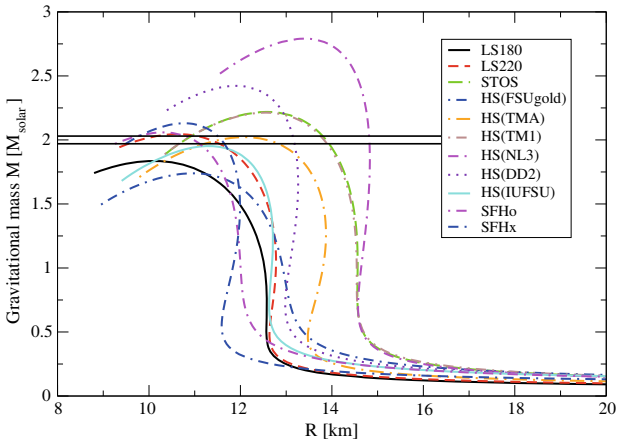


**Fig. 4.** Solutions of the TOV equations for a selection of EoS adopted from [34]. The selection illustrates mass-radius predictions by a variety of mean field models, non-relativistic (LS180, LS220) and relativistic (HS(FSUGold), HS(TMA), HS(TM1), HS(NL3), HS(DD2), HS(IUFSU), STOS(TM1), SFHo and SFx). Horizontal solid lines indicate the region (including errors) of heaviest observed neutron star masses. For more detail see the reference and text.

### 3.2 Simultaneous determination of mass and radius of the same object

The main methods used in determination of neutron star mass and radius involve data on transient low mass X-ray binaries (LMXB), or X-ray photospheric radius expansion (PRE) in Type-I X-ray bursts [35–39], or surface thermal emission spectra from stars in quiescent LMXB (see *e.g.* [40–44]). The distance of the star is also required. This can be relatively well estimated for stars in globular clusters, however, restriction to clusters limits the number of candidate stars. In other cases, the distance has to be inferred indirectly but the error of the results is significantly increased. Data analysis to extract masses and radii is rather involved [35] and new effects, which need to be taken into account, are being discovered. Recent spectral

**Table 2.** Selected estimates of mass and radius from data on Type-I X-ray bursts in transient LMXB and thermal emission from neutron star surface in quiescent LMXB, reported after 2010. For more details about the method of analysis and observational data see references.

| Radius [km] | $M/M_\odot$ | Confidence level % | Sources | Reference |
|---|---|---|---|---|
| 11–12 | 1.4 | | EXO 1745–248 | Steiner *et al.* 2010 [40] |
| | | | 4U 1608–522 | |
| | | | 4U 1820–30 | |
| | | | X7 (47 Tuc) | |
| | | | $\omega$ Cen | |
| | | | M13 | |
| $> 14$ | $< 2.3$ | | 4U 1724–307 | Suleimanov *et al.* 2011 [38] |
| $\leq 12.5$ | $\leq 2.1$ | | KS 1731–260 | Ozel *et al.* 2012 [45] |
| 7.6–10.4 | Mass | 90 | $\omega$ Cen | Guillot *et al.* 2013 [41] |
| | independent | | M13 | |
| | | | NGC 6397 | |
| | | | NGC 6304 | |
| | | | M28 | |
| | 1.4 | 90 | $\omega$ Cen | Lattimer and Steiner 2014 [42] |
| 11.15–12.66 | Basic EoS | | M13 | |
| 10.45–12.45 | Exo EoS | | NGC 6397 | |
| | | | NGC 6304 | |
| | | | M28 | |
| $> 13$ | 1.2–2.4 | | 4U 1608–52 | Poutanen *et al.* 2014 [39] |
| 9–14 | 1.4 | | X5 (47 Tuc) | Heinke *et al.* 2014 [44] |
| | $> 1.8$ | | X7 (47 Tuc) | |
| | (1.4) | | | |
| 10.1–11.1 | $\sim 1.5$ | | 4U 1820–30 | Ozel *et al.* 2015 [46] |
| | | | SAX J1748.9–2021 | |
| | | | EXO 1745–248 | |
| | | | KS 1731–260 | |
| | | | 4U 1608–52 | |

measurement of Type-I X-ray bursts [39] revealed strong dependence of the burst properties on the flux and spectral hardness of the persistent emission before burst which affects the extracted mass-radius information. Uncertainty as to effects of the composition of the stellar atmosphere and any absorbing material along the line of sight is a problem. This is one of the main reasons for differences in the results reported by several groups based on the same observational data (see table 2).

### 3.3 Neutron star cooling

The cooling of a neutron star in different phases of its life is one of the important pieces of observational information leading to constraints on neutron star theories.

We discuss here the history and outcome of the recent reports of rapid cooling of an isolated neutron star (referred to as Cas A) in the Cassiopeia A supernova remnant [47]. This example illustrates the complexity of observation and analysis of cooling data, yielding results that are subject to calibration and systematic uncertainties and ambiguous interpretation.

Heinke and Ho [48] analyzed X-ray spectra of Cas A taken during 2000–2009 by the ACIS-S detector in Graded mode on the Chandra X-ray observatory to obtain data on thermal evolution of Cas A. They reported a decline in the surface temperature of $3.6 \pm 0.6\%$ over nine years, suggesting unusually fast cooling. Shternin *et al.* [49] added another point to the data, taken and analysed in the same way as in [48], consistent with the trend discovered by Heinke and Ho. Elshamouty *et al.* [50] tested the decline in the effective temperature of Cas A using *all* Chandra detectors (ACIS and HRC types) and modes, using a more recent (2013) calibration. They added a new (2012) point

to the ACIS-S Graded mode observation results. They found that the ACIS-S Graded data indicated a temperature decay of 3.1%–5.0% over 10 years, with a best-fit decay of $3.5\% \pm 0.4\%$. In contrast, data collected by the HRC-S detector yielded 0.9%–2.0% decline over 10 years, with a best-fit decay of $1.0\% \pm 0.7\%$. The analysis of this data showed some dependence on the choice of source and background extraction regions. The combination of all data indicated a decline of $2.9\% \pm 0.5\%_{\rm stat} \pm 1.0_{\rm sys}\%$ over 10 years. Elshamouty *et al.* stressed the complexity of the bright and varying supernova remnant background that made definitive interpretation of Cas A Chandra observations difficult.

The ACIS-S Graded mode observations are known to be subject to spectral distortions because of pile-up and charge transfer inefficiency effects. Consequently Posselt *et al.* [51] performed dedicated observations in 2006 and 2012 using the ACIS in the Faint telemetry mode where the instrumental effects were minimized. Extensive analysis of the data was made, with examination of many possible effects which could affect the thermal emission. These included variation in parameters of star atmosphere models, changes in the magnitude of the emission areas and instrument calibration issues. The authors concluded: *Overall, our results from 2006 and 2012 are consistent with no temperature decline at all, or a smaller temperature decline than that reported for the data suffering from pile-up and acquired in Graded mode during the time interval from 2000 to 2012.*

The next two points in the set of effective temperature measurements were added in 2013 and 2014 from ACIS-S Graded observations by Ho *et al.* [52] and showed consistency with the reported rapid cooling followed since 2000. However, Posselt *et al.* [53] discussed in detail calibration and contamination issues with ACIS detectors. They reported *preliminary* new 2015 data point, still under analysis, obtained in a similar way as the 2006 and 2012 points in [51] that were consistent with no significant change in temperature. The new 2015 point seems to suggest a drop in temperature $\Delta T = (-0.27 \pm 0.21) \times 10^4$ K per year, still consistent with no rapid cooling.

The cooling history of Cas A has stimulated extensive theoretical effort to explain the data, mainly based on the assumption of existence of neutron superfluidity and proton superconductivity in the interior of the star. Detailed description of the theory goes beyond the scope of this review and thus we make only a few general comments.

There are two main types of models. The "minimal cooling scenario" [54] explains enhanced cooling in a particular epoch of the onset of baryon superfluid state. Superfluidity reduces emissivity of the usual neutrino reactions and introduces a specific "Cooper pair breaking and formation" neutrino emission mechanism. In general, the Cooper pair formation releases energy which can be taken away by a neutrino-antineutrino pair, thus increasing neutrino emissivity. The minimal cooling scenario, although formally successful in explaining the Cas A cooling [48] has, however, a serious drawback. It does not include "medium (collective) effects" which become significant in high density matter and account for changes in nucleon-nucleon interactions due to the presence of other nucleons in the matter. These significantly affect neutrino emissivity, superfluid gap values, thermal conductivity and related influences governing neutron star cooling (*e.g.* [55–57] and references therein).

There are two issues that should be addressed in future development of the superfluidity based models. First, as recently emphasized by Ho *et al.* [52], a single theory which would provide the superfluid and superconductor gap energies and the EoS of the neutron star interior is not available at present. In other words, the gap energies and the EoS used to describe other properties of neutron stars, are mutually inconsistent. Second, a more speculative question, relates to uncertainty concerning the interiors of neutron stars. Most of the models based on superfluidity require substantial presence of neutrons and protons in the neutron star cores. The densities and composition of the cores are not known directly from observation, but are inferred in a model-dependent way. The currently accepted central particle number densities are in the region of $\sim$ 3–6 $\rho_0$. A question arises whether one can regard nucleons at that density as keeping their identity and behavior as at normal nuclear density or whether the unavoidable overlap in high density matter affects their internal structure and properties. In addition, would the other constituents of the matter, such as hyperons or quarks, influence the cooling in any way?

Finally, for completeness, we mention other models, besides the onset of superfluidity and superconductivity, invoked to explain cooling of Cas A, summarized in [52]. They include transition to quark phases [58, 59], magnetic field decay [60] and heating by r-mode oscillations [61]. Identification of observational fingerprints that distinguish between the models, and, indeed, clarification of the cooling data for Cas A, remains a challenge for the future.

## 4 Terrestrial constraints

### 4.1 Heavy-ion collisions

Heavy-ion collisions are the only terrestrial events in which hot high-density matter is created. The beam energies range from $\sim 35$ MeV to $\sim 5$ TeV per nucleon, specific to different facilities such as NSCL, Texas A&M, GSI, RHIC and LHC (existing), and FAIR and NICA (future).

At beam energies $\sim 35$ MeV–2 GeV per nucleon, which access the region below nuclear density and temperatures up to several tens of MeV, neutron/proton spectral ratios and nucleon and light fragment flows can been studied [62]. One of the important results of such experiments is thought to be information on the nuclear symmetry energy and its density dependence. The data are used to fit parameters of transport models, which in turn provide energy density and pressure in the matter, *i.e.* the EoS [63–67]. The much-discussed question arises whether such EoS can be meaningfully used to constrain the EoS of high-density matter in neutron stars and supernovae.

At this range of beam energies used in experiments with Au or Sn projectiles inelastic (N-N) scattering may

**Table 3.** Comparison of basic properties of (a) matter created in heavy ion collisions (HIC) with beam energies $< 1\,\mathrm{GeV}$ per nucleon and (b) matter in proto-neutron stars (PNS) for progenitor stars of 8–20 $M_\odot$. S, B, L stands for strangeness, baryon and lepton number, respectively. N and N$^*$ are N – baryons (nucleons) and their resonances, $\Delta$, $\Delta^*$ are $\Delta$ – baryons and their resonances. $\rho_0$ is normal nuclear density, $0.16\,\mathrm{fm}^{-3}$.

| | HIC | PNS |
|---|---|---|
| Temperature | $< 50\,\mathrm{MeV}$ | $< 50\,\mathrm{MeV}$ |
| Energy density $\epsilon$ | $\sim$ 1–2 $\mathrm{GeV/fm}^3$ | $\sim 1\,\mathrm{GeV/fm}^3$ |
| Baryon density $\rho$ | $< 2.5\ \rho_0$ | 2–3 $\rho_0$ |
| Time scale to cool down | $10^{-23}$ to $10^{-24}$ s | 1–10 s |
| | | $\rho$ and $T$ dependent |
| Interaction | Strong | Strong and Electro-Weak |
| | S, B, L conserved | B, L conserved |
| Composition: | N, N*, $\Delta$, $\Delta^*$ | n, p |
| | $\pi$, (K) | no pions |
| | strangeness rare | strange baryons and mesons |
| | no leptons | copious leptons |
| Symmetry: | close to symmetric | highly asymmetric |
| Thermal equilibrium | possibly local | yes |

becomes significant and matter consists mostly of N, N$^*$, $\Delta$, $\Delta^*$ and light nuclear fragments such as $^3$H, $^3$He, $^4$He, $^7$Li, $^7$Be and pions. Strangeness becomes less important, but kaons may be expected [67]. It is claimed that, for a small fraction of the time, number densities as high as 5 times nuclear saturation density $\rho_0$ [62, 65], can be achieved in $^{197}\mathrm{Au} + {}^{197}\mathrm{Au}$ collisions due to inertial confinement. After the collision, the matter cools fast from an initial $T \sim 50\,\mathrm{MeV}$ and dilutes to subnuclear densities.

Theoretical approaches to the dynamics of heavy ion collisions at medium energies are either algebraic, based on self-consistent solution of the Boltzmann equations used in transport models (see *e.g.* [63–65, 68]), or geometric, using molecular dynamics simulation in which particles are treated as Gaussian wave packets in a unit cell [68–70]. Both classes of theories yield predictions on trajectories of particles emitted from the collision region. In addition, the molecular dynamics models provide information on emission of clusters.

Without going into details of the application of these models of the collision to actual data, there are several open questions in interpretation of the results and their implications for understanding of the structure of high-density matter. It is true, that after extrapolation to low temperature, the heavy ion collision theories can produce constraint on the EoS of the symmetric nuclear matter. However, constraints extracted from heavy ion collision experiments are not applicable to matter in cold neutron stars and core-collapse supernovae. The composition of the matter in these astrophysical objects is not the same as of the matter created in heavy ion collisions and the EoS will be different. To make this important point clear, we contrast basic properties of the two scenarios in table 3.

Matter created at higher beam energies has typically very low particle number density (significantly lower than the saturation density of the symmetric nuclear matter), but relatively high energy density 1–6 $\mathrm{GeV/fm}^3$ (dependent on beam energy) and close to zero baryon chemical potential. The matter is heated to several hundred MeV. The time-scale between the collision and the chemical and thermal freeze-out is of order $10^{-23}$ to $10^{-24}$ s which implies that the creation of particles during the collision is governed only by the strong interaction. This has the important consequence that only processes that conserve strangeness and baryon and lepton number can occur. Analysis of particle spectra and ratios indicate that quark-gluon plasma may be reached and quark-antiquark pairs, strange baryons and mesons, pions, and a significant number of their antiparticles are subsequently created. The matter is lepton poor, in particular containing very few neutrinos.

The focus of high beam energy experiments is a search for quark-gluon plasma and the hadron-quark matter transition. The latter could have an important consequence for core-collapse supernova physics, if found at relevant temperatures and densities.

### 4.2 Hypernuclei

Realistic models of neutron star matter need to include hyperons at central densities exceeding 2–3 times nuclear saturation density. Thus it is important to model N-Y and Y-Y forces, acting in the nuclear environment, as well as possible. Experimental study of hypernuclei is the only direct source of information on these forces. The argument that hyperons should play a role in the structure of neutron stars is quite compelling. Because of the Pauli principle, the chemical potential for neutrons rises rapidly with increasing density, reaching that for $\Lambda$ hyperons at (2–3) $\rho_0$. It then becomes energetically favourable for the system to let the neutrons undergo a strangeness changing

weak decay, which replaces them by hyperons for which the Fermi sea is not yet filled, thus lowering the total energy of the system. As strangeness is not conserved on the weak interaction time-scale and the time-scales for neutron star formation are much greater than those associated with weak interactions, the growth of strangeness will continue until equilibrium is reached. This means that any hyperon energetically allowed must appear. Rather than being a surprise to find hyperons it would stretch our understanding of fundamental strong and weak interaction processes to breaking point if they were not to appear. It is certainly inconceivable that a nucleon-only EoS could be realistic at such large densities.

The study of $\Lambda$ hypernuclei has a long history, with shell structure mapped out across the periodic table [71–76]. Systematic studies of the energy levels of light $\Lambda$ hypernuclei have enabled extraction of considerable detail concerning the (mostly) attractive effective $\Lambda$N interaction.

As for $\Sigma$ and $\Xi$ hypernuclei, the situation is quite different. The special case of $^4$He aside, there is no experimental evidence for any $\Sigma$ hypernuclei [77–79], despite extensive searches. Indeed, it seems likely that the $\Sigma$-N interaction is somewhat repulsive and that there are no bound $\Sigma$ hypernuclei beyond $A = 4$. In the case of the $\Xi$, the experimental situation is very challenging, with just a handful of observations of doubly strange nuclei. Very recently the long-awaited experimental result on $\Xi^-$ hypernucleus was published [80] suggesting that the $\Xi$-nucleus potential is substantially attractive. This result supports the prediction of the QMC model (see sect. 5 which finds the threshold for $\Xi$ population at densities close to that of $\Lambda$ hyperons and lower than the threshold for appearance of $\Sigma$ hyperons in cold, $\beta$-equilibrated neutron star matter).

### 4.3 Lattice QCD

It would be desirable to test predictions of many theories against results obtained in lattice quantum chromodynamics. As the only adjustable-parameter-free theory currently available, it can be regarded as a numerical experiment [1], with a potential to understand high-density matter in compact objects from first principles.

Lattice QCD is a non-perturbative approach to solving the quantum chromodynamics theory of quarks and gluons, formulated on a grid or lattice of points in space and time. At present, predictions of lattice QCD are available only for fermionic systems in free space - at zero density and high temperature. The reason for preventing its application in theories involving non-zero density of strongly interacting fermions lies in a numerical difficulty called the *sign problem*. The problem generally arises in Quantum Monte Carlo simulations of any system of interacting fermions, because their wave functions change sign when any two fermions are interchanged (due to Pauli principle) [81]. Unless there are exact cancellations, the quantum-mechanical sum over all multi-particle states of the system involves an integral over a function that is highly oscillatory, and hence hard to evaluate numerically, particularly in high dimensions.

In lattice QCD the expectation value of any physical observable is represented by a path integral over all quark and gluon fields configurations, which is evaluated using the Monte Carlo method. At finite density (or, equivalently, finite chemical potential) and low temperatures the evaluation of the path integral fails because of the near-cancellation of the positive and negative terms that cannot be calculated with sufficient accuracy. More technical description of the sign problem in QCD goes beyond the scope of this paper, but we refer interested reader to, *e.g.* [81–83].

Because of this problem, it is questionable whether the lattice calculation can be ever extended to finite densities although many attempts have been made in the past, and some promising steps are currently being made (see *e.g.* [84]). If lattice QCD were to eventually provide data directly aiding determination of the EoS of high-density matter it would be a significant step forward.

## 5 Quark-Meson-Coupling (QMC) model

It has become apparent in previous sections that currently available observational and experimental data are not yet adequate to uniquely constrain the EoS of high-density matter. We suggest that, along with the need for more precise data, a principle aim for theorists should be to develop new and improved theories in which parameters are directly related to microphysical quantities for which good estimates can be made. In this section we bring an example of a theory of this type which has not hitherto received much attention.

Conceptually, one of the main difficulties in solving the nuclear many-body problem is to incorporate medium effects into the calculation. In contrast to, for example, elementary quantum electrodynamics, where the force between two electric charges is quantified by the Coulomb law and forces among many electrons can be calculated precisely using the principle of superposition, no equivalent approach exists in nuclear physics. Scattering experiments with free nucleons provide information about bare N-N potentials, but an involved numerical treatment is necessary to transform these potentials to a describe adequately the forces between hadrons in the hadronic environment.

The idea of modeling the N-N interaction using quark degrees of freedom originated in the late 1980s with Guichon [85] and Guichon and Thomas [86] who suggested that the origin of nuclear many body forces and of the saturation of nuclear forces can be found in the modification of the structure of a nucleon when it is imbedded in a medium consisting of other nucleons. The model, referred to as the Quark-Meson-Coupling (QMC) model, has been adopted and developed in different forms in Australia, Japan, China, Korea, Brazil and Europe [87].

The basic assumption of the QMC model is that, instead of the usual treatment of modeling nuclear forces through exchange of mesons coupled to nucleons, taken as

point-like particles, this exchange takes place directly between quarks in different non-overlapping nucleons, taken as having a structure in the form, for example, of the MIT bag. It is the mutual interaction between the quark and meson fields, which leads to the saturation property of nuclear forces [85].

The bag model is taken as an effective realization of confinement, which must not be taken too literally. The lattice QCD simulations of Bissey *et al.* [88] indicate that the true confinement picture is closer to a T-shaped color string attached to the quarks. Outside this relatively thin string one has the ordinary, non-perturbative, vacuum, where the quarks from other hadrons can pass without disturbing the structure very much. So, even though the bag model imposes a strict condition which prevents the quarks from travelling through its boundary, this must be seen as the average representation of a more complex situation and one should not attribute a deep physical meaning to the surface of the bag nor to its size. In particular, estimating the density at which the QMC approximation breaks down as the reciprocal of the bag volume is certainly too mechanical [89]. Of course, there is a density above which such models become inadequate, but it is safe [89] to assume that this critical density is large enough that we can use the model to predict the properties of neutron stars.

All variants of the QMC model, rather than starting with the bare N-N force, begin with the concept of a nucleon, modeled by the MIT bag, immersed in a nuclear medium. The effects of the coupling to the $u$ and $d$ quarks of a scalar-isoscalar meson ($\sigma$) mean field, generated by all the other nucleons in the medium, on the internal structure of that nucleon are then included self-consistently. As in earlier boson-exchange models, the $\sigma$ is a crude but convenient way to simulate the effects of correlated two-pion exchange between hadrons. The quarks are also coupled to $\omega$ and $\rho$ mesons, which, at least at the Hartree level, simply shift quark energies.

Assuming [85] that the nucleon is located in average, time independent, meson fields $\bar{\sigma}$, $\bar{\omega}$ and $\bar{\rho}$, the MIT bag equations are solved to obtain the expression for the quark field, depending on the quark-meson coupling constants $g^q_\sigma$, $g^q_\omega$ and $g^q_\rho$, the free nucleon radius $R_0$ and the vacuum energy density $B$, adjusted to yield the mass of the free bag equal to the spin-isospin averaged mass of the nucleon and the $\Delta$. Of the coupling constants, only $g^q_\sigma$ is density dependent. These quark-meson couplings describe the interaction between quarks in *different* hadrons. They act as the source of mean fields in medium as well as serving to modify the equation of motion of the confined quarks. This leads to a *self-consistency* problem, which is highly non-trivial for the scalar field. As a result, the effective strength of the coupling of the scalar meson to a hadron containing light quarks is suppressed as the scalar field increases, or equivalently, as the density increases.

In this self-consistent calculation at the quark level, one can express the in-medium nucleon masses $M_{\rm eff}(\bar{\sigma})$, given as a function of the scalar field, through a calculated, density-dependent, scalar coupling,

$$M_{\rm eff}(\bar{\sigma}) = M - g_{\sigma N}\bar{\sigma} + \frac{d}{2}(g_{\sigma N}\bar{\sigma})^2, \tag{4}$$

where $d$ is the scalar polarizability of the nucleon. This scalar polarizability is an essential feature of the QMC model and is related to the bag radius $R_{\rm B}$ as $d = 0.0044 + 0.211R_{\rm B} - 0.0357R^2_{\rm B}$. A simple relation relates the quark-meson coupling constants to the nucleon-meson constants

$$g_{\sigma N} = 3g^q_\sigma \int_{\rm Bag} {\rm d}\boldsymbol{r}\bar{q}q(\boldsymbol{r}), \qquad g_{\omega N} = 3g^q_\omega, \qquad g_{\rho N} = g^q_\rho, \tag{5}$$

where $q$ is the valence quark wave function for the MIT bag. The influence of nucleon substructure, in a mean-field approximation, is entirely described in terms of the parameterization of the effective mass of the nucleon through the density-dependent scalar coupling derived from the quark model of the nucleon and $g^q_\sigma$. Therefore the explicit description of the internal structure of the nucleons can be replaced by constructing an effective relativistic Lagrangian on the hadronic level, with the calculated non-linear $\sigma$-nucleon couplings and proceeding to solve the RMF equations in a standard way.

The scalar polarizability describes the self-consistent response of the nucleon to the applied mean scalar field which tends to oppose that applied field. By analogy with the electric polarizability of an atom, which tends to arrange its internal structure to oppose an applied electric field, the effective $\sigma$-N coupling reduces as the surrounding $\sigma$ field increases. This mechanism is the origin of saturation of nuclear forces in the QMC model. The scalar polarizability is a calculated property of the nucleon and hence introduces no new parameters into the model. Moreover, it is this scalar polarizability which yields the density dependence of the derived N-N effective force, or equivalently the three-body forces among nucleons.

The outline of the essential features of the QMC model has been presented so far for nucleons. However, it is directly applicable to any hadrons [76, 85, 86]. That is, the model predicts the existence and strength of the two- and three-body forces between not just nucleons, but nucleons and hyperons and hyperons and other hyperons, without additional parameters.

The essential feature of the QMC model is that it depends only on three well-defined and constrained adjustable parameters, the free nucleon-meson coupling constants $g_{\sigma N}$, $g_{\omega N}$ and $g_{\rho N}$. It is customary to define

$$G_\sigma = \frac{g^2_{\sigma N}}{m^2_\sigma}, \qquad G_\omega = \frac{g^2_{\omega N}}{m^2_\omega}, \qquad G_\rho = \frac{g^2_{\rho N}}{m^2_\rho}. \tag{6}$$

Their values are adjusted to reproduce the binding energy and the asymmetry energy coefficient of ordinary nuclear matter at the saturation point. The other parameter is the bag radius constrained to lie between 0.8 and 1.0 fm. The $\omega$ and $\rho$ meson masses and the isoscalar and isovector magnetic moments, [76, 91–93], are taken at their physical values. The $\sigma$ meson mass and its very existence as a particle is not completely clear as yet. It is usually identified

with the $\pi$-$\pi$ resonance, which has a wide decay width, observed in scattering experiments. The best $M\_\sigma$ estimate lie between 650 and 750 MeV, consistent with applications in other areas (see *e.g.* [76, 90, 109] and references therein). All the other elements of the model are calculated within the model or determined by symmetry. Consistent with the requirement for improved theory, all the parameters of the QMC model have physical meaning and cannot be varied outside well-defined boundaries.

One persistent feature of the QMC models is that they predict a value of the incompressibility of symmetric nuclear matter at saturation, $K_0$, in the range 280 to 350 MeV. This value is somewhat higher than the value which has been prevalent for many years. In the light of the recent re-analysis of data on giant monopole resonances [94], which finds $250 < K_0 < 315$ MeV, the QMC predictions are acceptable.

### 5.1 Application of the QMC model to nuclear matter and neutron stars

The performance of the QMC model as concerning the EoS of high-density matter and neutron stars has been studied in [89]. Similar results have been obtained, with a slightly variant version of the model in [87, 95–97]. The main results, obtained with the QMC700 EoS, are compared with results from APR [21], SkM* [98] and the Bethe-Johnson (BJ) model [99]. APR and SkM* are chosen as widely used representatives of nucleon-only realistic potential and non-relativistic mean-field models. APR, based on A18+v+UIX*, the Argonne18 N-N potential a relativistic boost and three-body forces, has over 20 parameters. The Skyrme parameterization SkM* is dependent on seven variable parameters. The BJ model includes $\Lambda$ and $\Sigma$ hyperons but the N-Y interaction is different from the QMC model.

The pressure dependence of the energy per particle of $\beta$-equilibrium matter, directly relevant for modelling of neutron stars, is presented in fig. 5. The left hand panel shows the QMC700 results. The full curve is the prediction for the complete model including the full baryon octet (F-QMC700), the dashed curve illustrates the result when only nucleons are present. In this model, the natural appearance of hyperons, which occurs at $\epsilon \sim 600\,\mathrm{MeV\,fm^{-3}}$, as expected softens the EoS. As we will see, this softening is vitally important in facilitating the existence of heavier neutron stars. In the right panel, the APR and SkM* results, being nucleon-only, show no softening. The BJ model results show behaviour broadly similar to F-QMC700, however there are differences in detail in the composition and threshold densities of the non-nucleon species.

However, the mechanism of softening of EoS is complex and variation of composition is not the only way to achieve it. The pressure also depends critically on the potentials acting between the particles present and, in turn, on the density dependence of the symmetry energy. Thus, for example, the SkM* Skyrme model produces a very soft EoS, in contrast to APR.

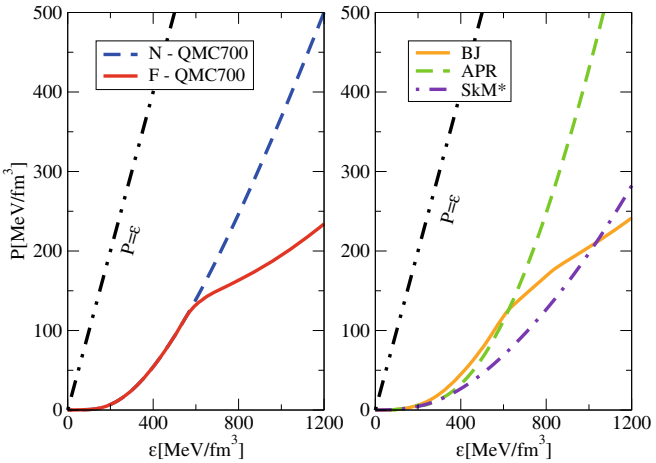


**Fig. 5.** Left panel: Pressure as a function of total energy density for sample EoS for $\beta$-equilibrium matter containing only nucleons and leptons p + n + e + $\mu$ (N-QMC700) and the full baryonic octet and leptons (F-QMC700). Right panel: Results of BJ (includes hyperons) and APR, SkM* (nucleon only) EoS. The curve $P = \epsilon$ shows the stiffest possible EoS. The kink in the $P$-$\epsilon$ curves represents the onset of hyperons in F-QMC700 and BJ EoS. For more details see text.

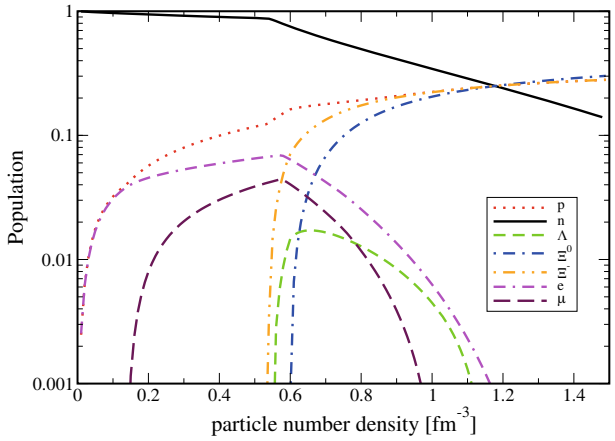


**Fig. 6.** Relative population of baryons and leptons in $\beta$-equilibrium matter for QMC700. For more explanation see [89].

The predictions of the threshold densities for appearance of hyperons, essential for description of high-density matter and neutron stars, differ in the QMC model from the other more conventional relativistic models. As shown in fig. 6, the QMC model predicts the onset of production of hyperons at densities about 3 times nuclear saturation density. Furthermore, the first hyperons to appear are the cascades, $\Xi$, together with the $\Lambda$ hyperon. The $\Sigma$ hyperons are not produced at densities below 1.2 fm$^3$. This scenario is a direct consequence of features which are present in the QMC model and absent in conventional relativistic field models (for details see [89]). As discussed in sect. 4.3, the QMC result for $\Sigma$ hyperons is supported by the fact that no bound $\Sigma$-hypernucleus at medium or high mass has been found as yet despite dedicated search. The appearance of the $\Xi$ hyperons at rather low densities indicates

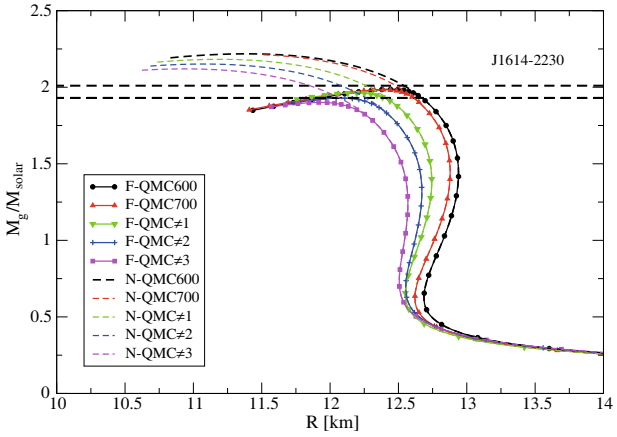


**Fig. 7.** The gravitational masses of non-rotating neutron-star models (measured in solar masses) plotted against radius (in kilometers), calculated in QMC with hyperons (F) and nucleon-only (N). The number in the curve label means the $\sigma$ meson mass and $\pi$ indicates models with $\pi$ meson included. The horizontal dashed lines depict the largest neutron star mass yet reported [32, 33]. For more explanation see text and ref. [89].

the existence of a bound $\Xi$-hypernucleus. This prediction is in line with the very recent results of Nakazawa *et al.*, who reported observation of a deeply bound state of the $\Xi^-$-14N system [80].

In traditional RMF models the sequence of appearance of hyperons with increasing density usually follows their masses, predicting the $\Lambda$ hyperon at lowest density, followed by $\Sigma$ and $\Xi$. They first appear at density around twice nuclear saturation density. In these models the strength of the N-Y interaction is not calculated, but fitted to data, imposed as a variable parameter or taken to be the same —or similar to— the N-N interaction. This uncertainty in the N-Y potential influences directly the density dependence of the hyperon population. As an example in [100, 101] we find two choices of the $U_\Sigma$ potential. When the $U_\Sigma$ potential was chosen to be negative (attractive), the lightest $\Sigma$ hyperon appeared at $\sim 0.75\,\mathrm{fm}^{-3}$, whereas a positive (repulsive) potential moves this threshold beyond densities relevant to cores of neutron stars. Taking the $U_\Xi$ potential to be attractive in both scenarios causes the predicted appearance of $\Xi$ hyperons at rather low densities, $\sim 0.4\,\mathrm{fm}^{-3}$, even lower than the QMC prediction.

The composition of matter at densities expected in the cores of neutron stars has a decisive consequence for the maximum mass of a cold neutron star. Appearance of hyperons effects the EoS as is seen clearly in fig. 7. Cold neutron stars with maximum masses in the range (1.99–1.90) $M_\odot$, depending on the details of the model, were predicted in QMC three years before their observation, assuming matter containing the full baryon octet (nucleons and hyperons) [89]. The ranges of corresponding radii, central densities and central pressures are (12.45–11.93) km and (1.66–1.74) $\times\, 10^{15}\,\mathrm{g/cm}^3$, [(6.61–6.93)$\rho_0$] and (182–209) MeV fm$^3$. The gravitational red shift is 0.38, in line with observational constraint [108], and the speed of sound is 0.66 $c$. We note that the central densities are well below the upper bound quoted in [32].

However, this version of the model does not predict neutron stars heavier than $\sim 2M_\odot$. Should such a star be observed, the QMC model published in [89] would fail. The physical constraints of the parameters do not allow their free variation to adjust the model prediction to new observational data. The failure would signal a lack of important physics in the model which would have to be sought after and included.

In fig. 7 we see clearly that the introduction of the full baryon octet considerably reduces the possible maximum mass. In traditional models this softening is much more significant and leads to the hyperon puzzle (see *e.g.* fig. 13 in [102]), *i.e.* the presence of hyperons in neutron star cores prevents existence of neutron stars as massive as the highest observed. Several remedies have been suggested to remove this difficulty, including introduction of three body Y-Y forces [103], application of the Auxiliary Field Diffusion Monte Carlo (AFDMC) model to study N-$\Lambda$ potentials [104], suggestion of hyperon mixing and universal many-body repulsion in neutron stars [105] or introducing an alternative theory of gravity [107]. The QMC model offers a simple solution of this puzzle in calculating the hyperon-nucleon consistently within its framework. We note that a heavy neutron star was also predicted in 2006 by Lackey *et al.* [108] in RMF models with a specific (empirical) choice of N-Y potentials.

### 5.2 Application of the QMC model to finite nuclei

One of the significant constraints on the QMC model is the requirement that it has to perform equally well in infinite matter (neutron stars) and finite nuclei. First nuclear investigations, reported by Guichon *et al.* [90], were limited to spherical nuclei at closed shells.

In a very recent development [109], QMC based calculation of a number of properties of open shell even-even nuclei across the entire periodic table, from $^{12}$C to $^{270}$Ds, including nuclei with quadrupole and octupole deformation, was performed. A non-relativistic approximation to QMC [90] was used to derive a density dependent effective force, hence making direct connection between the treatment of nuclear structure and the underlying quark model (and perhaps eventually QCD itself) [86, 90, 110]. A key feature of this force is the novel form for the density dependence involving inverse powers of $(1 + d\rho G_\sigma)$ (with $G_\sigma = g^2_{\sigma N}/m^2_\sigma$ and $g_{\sigma N}$ the $\sigma$-nucleon coupling constant at zero density). It is the self-consistent rearrangement of the internal structure of the nucleon in medium, represented by the scalar polarizability, that gives rise to the density dependence (or equivalently the many-body forces).

We recall that the model depends on only four parameters (three coupling constants and the choice of mass of the $\sigma$ meson) which are severely limited in their range. Yet it produces overall agreement with experimental data of a quality comparable to successful Skyrme forces which

have with more parameters which lack physical content and cannot be uniquely determined. When extended beyond the region of data used to obtain the best values within the limited allowed range, the QMC force provides an excellent description of diverse data. These include the ground state binding energies and quadrupole deformations of super-heavy nuclei ($100 \leq Z \leq 110$ and $146 \leq N \leq 160$), the evolution of quadrupole deformation across isotopic chains including shell closures, the shape co-existence between prolate, spherical and oblate shapes in the Zr region and the double quadrupole-octupole phase transition in the Ra-Th region. As an example of the success of the QMC model, we show in fig. 8 results of the calculation of binding energies and quadrupole deformations of 15 super-heavy nuclei in comparison with calculations using a Skyrme force SV-min [111] and Finite-Range-Droplet model (FRDM) [112]. It is interesting to note that all Skyrme like models predict under-binding of super-heavy nuclei and, in contrast, relativistic mean field models overbind these nuclei. This phenomenon has been discussed by Reinhard *et al.* [113], but it is not yet fully understood in FRDM and QMC models.

These features suggest that this new force may serve as a powerful tool for nuclear astrophysics and general low energy nuclear structure studies of relevance to the many rare-ion beam facilities operating or under construction.

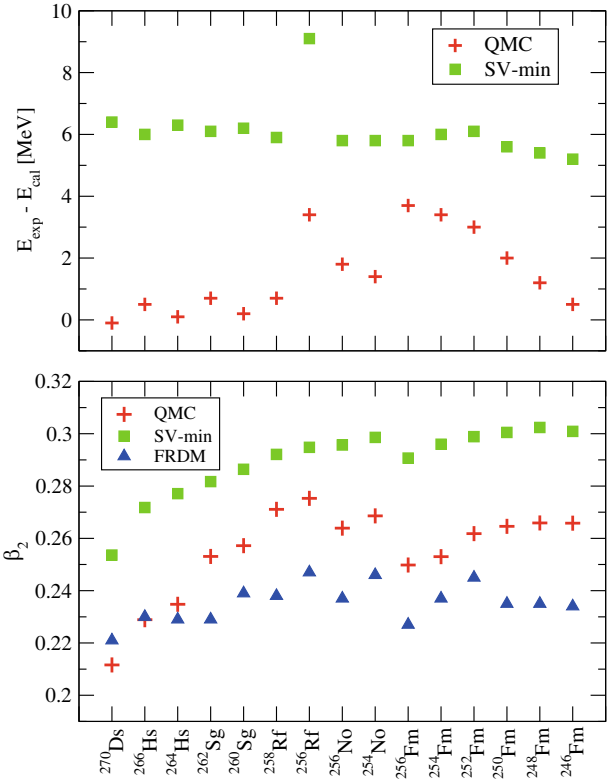


**Fig. 8.** Difference between calculated and experimental binding energies of superheavy elements as obtained with QMC and SV-min forces (top panel). Quadrupole deformation parameters $\beta_2$ are also shown and compared with predictions of FRDM [112] (bottom panel).

## 6 Summary and conclusions

The main purpose of this paper has been to critically assess the current status of knowledge of the properties of high-density matter at and above nuclear saturation density, with a particular focus on the interior of neutron stars. Although there is some evidence for constraining the EoS, particularly of pure neutron matter, below that density, there is great uncertainty as to what happens at higher densities. Available astrophysical observational data, as well as data from terrestrial experiments, have insufficient accuracy and sensitivity to the microscopic make-up of the matter to provide information to allow construction of a meaningful, well-based, EoS.

We focused on the most relevant input data, *viz.* neutron star masses, the simultaneous determination of masses and radii, and the cooling properties of neutron stars. Gravitational waves, although they may eventually make a significant contribution, are as yet unobserved.

The most prominent terrestrial experiments, heavy-ion collisions, suffer from a significant model dependence in their analysis and are in any case not providing information relevant to the high-density, low-temperature $\beta$ equilibrium interior of neutron stars. Other terrestrial methods, including parity violating electron scattering, antiprotonic atoms and determination of the electric dipole strength function (see review, *e.g.* [62]) have similar problems, yielding information of limited relevance to EoS in stellar environments.

Current mainstream theoretical approaches to high-density matter have many (correlated) parameters generally lacking clear physical meaning. The number of equivalent parameter combinations is practically infinite. Any time a new piece of experimental data appears, in too many theoretical models there is freedom by parameter adjustment to obtain agreement with the data. But does this represent progress? Successul description of the new data by a model with already fixed parameters is a better objective. Development of models for only local application having very limited or no predictive power in related phenomena is of little value.

We anticipate progress on both experimental and theoretical fronts. On the astrophysics side, the new, now approved, NICER (The Neutron star Interior Composition ExploreR) [114] NASA mission promises to "*explore the exotic states of matter inside these stars, where density and pressure are higher than in atomic nuclei, confronting theory with unique observational constraints. NICER will enable rotation-resolved spectroscopy of the thermal and non-thermal emissions of neutron stars in the soft* (0.2–12 keV) *X-ray band with unprecedented sensitivity, probing interior structure, the origins of dynamic phenomena, and the mechanisms that underlie the most powerful cosmic particle accelerators known*". In addition, any signal from gravitational wave detectors would be most desirable [115]. On the terrestrial side, the FAIR and NICA accelerators can be expected to shed new light on the composition of matter created in heavy-ion collisions.

Finally, as an example of theoretical concepts alternative to the status quo, we gave space to a Quark-Meson-Coupling model, which has not hitherto received a lot of attention. Yet, it offers theoretical insight into medium effects on the structure of individual hadrons and the origin of many-body forces in matter over a usefully wide density range. Both effects are not well understood in current many-body models. The strongly attractive feature of the model is the limited number of parameters, well connected to physics and strongly constrained. Since there is no room to arbitrarily vary parameters in this model, any disagreement with new data indicates physics beyond the existing framework.

The extreme conditions of high-density matter stretch both theory and experiment to their limits. Even partial solution of the challenges would constitute real progress in our understanding of Nature.

## References


1. W. Weise, Prog. Part. Nucl. Phys. **67**, 299 (2012).
2. F. Weber, Prog. Part. Nucl. Phys. **54**, 193 (2005).
3. M.G. Alford, Nucl. Phys. A **830**, 385c (2009).
4. D. Blaschke, F. Sandin, T. Klahn, J. Berdermann, Phys. Rev. C **80**, 065807 (2009).
5. A. Chodos, R.L. Jaffe, K. Johnson, C.B. Thorn, V.F. Weisskopf, Phys. Rev. D **9**, 3 (1974).
6. T.A. DeGrand, R.L. Jaffe, K. Johnson, J.E. Kiskis, Phys. Rev. D **12**, 2060 (1975).
7. S. Weissenborn, I. Sagert, G. Pagliara, M. Hempel, J. Schaffner-Bielich, Astrophys. J. Lett. **740**, L14 (2011).
8. Y. Nambu G. Jona-Lasinio, Phys. Rev. **122**, 345 (1961).
9. M. Buballa, Phys. Rep. **407**, 205 (2005).
10. H.J. Pirner, G. Chanfray, O. Nachtmann, Phys. Lett. B **147**, 249 (1984).
11. D. Logoteta, I. Bombaci, C. Providencia, I. Vidana, Phys. Rev. D **85**, 023003 (2012).
12. H. Chen, M. Baldo, G.F. Burgio, H.-J. Schulze, Phys. Rev. D **86**, 045006 (2012).
13. H. Chen, J.-B. Wei, M. Baldo, G.F. Burgio, H.-J. Schulze, Phys. Rev. D **91**, 105002 (2015).
14. A. Kurkela, P. Romatschke, A. Vuorinen, Phys. Rev. D **81**, 105021 (2010).
15. E.S. Fraga, A. Kurkela, A. Vuorinen, Astrophys. J. Lett. **781**, L25 (2014).
16. A. Kurkela, E.S. Fraga, J. Schaffner-Bielich, A. Vuorinen, Astrophys. J. **789**, 127 (2014).
17. M. Dutra, O. Lourenco, J.S.Sa. Martins, A. Delfino, J.R. Stone, P.D. Stevenson, Phys. Rev. C **85**, 035201 (2012).
18. M. Dutra, O. Lourenco, S.S. Avancini, B.V. Carlson, A. Delfino, D.P. Menzes, C. Provindencia, S. Typel, J.R. Stone, Phys. Rev. C **90**, 055203 (2014).
19. Z.H. Li, U. Lombardo, H.-J. Schulze, W. Zuo, L.W. Chen, H.R. Ma, Phys. Rev. C **74**, 047304 (2006).
20. Z.H. Li, H.-J. Schulze, Phys. Rev. C **78**, 028801 (2008).
21. A. Akmal, V.R. Pandharipande, D.G. Ravenhall, Phys. Rev. C **58**, 1804 (1998).
22. T. Kruger, I. Tews, K. Hebeler, A. Schwenk, Phys. Rev. C **88**, 025802 (2013).
23. M.G. Alford, S. Han, M. Prakash, Phys. Rev. D **88**, 083013 (2013).
24. M.G. Alford, S. Han, Eur. Phys. J. A **52**, 62 (2016) arXiv:1508.01261v1, contribution to this Topical Issue.
25. C. Roberts, *talk at 2nd Workshop on Dense Matter from Chiral Effective Theories (DM15) 24-28 June 2015, Jilin University*, Chang-chun, Jilin, China.
26. S. Benic, D. Blaschke, D.E. Alvarez-Castillo, T. Fischer, S. Typel, Astron. Astrophys. **577**, (2015) A40 (2015).
27. N.K. Glendenning, C. Kettner, Astron. Astrophys. **353**, L9 (2000).
28. A.W. Steiner, J.M. Lattimer, E.F. Brown, Astrophys. J. Lett. **765**, L5 (2013).
29. A.G. Lyne *et al.*, Science **303**, 20 (2004).
30. R.A. Hulse, J.H. Taylor, Astrophys. J. Lett. **195**, L51 (1975).
31. P.C.C. Freire *et al.*, Mon. Not. R. Acad. Sci. **412**, 2763 (2011).
32. P. Demorest, T. Pennucci, M.S.E. Roberts, W.T. Hessels, Nature **467**, 1081 (2010).
33. J. Antoniadis *et al.*, Science **340**, 448 (2013).
34. T. Fischer, M. Hempel, I. Sagert, Y. Suwa, J. Schaffner-Bielich, Eur. Phys. J. A **50**, 46 (2014).
35. C.O. Heinke, J. Phys.: Conf. Ser. **432**, 012001 (2013).
36. D.K. Galloway, M.P. Muno, J.M. Hartman, D. Psaltis, D. Chakrabarty, Astrophys. J. Suppl. **179**, 360 (2010).
37. F. Ozel, D. Psaltis, Phys. Rev. D **80**, 103003 (2009).
38. V. Suleimanov, J. Poutanen, M. Revnivtsev, K. Werner, Astrophys. J. **742**, 122 (2011).
39. J. Poutanen, J. Nattila, J.J.E. Kajava, O.-M. Latvala, D. Galloway, E. Kuulkers, V. Suleimanov, Mon. Not. R. Acad. Sci. **442**, 3777 (2014).
40. A.W. Steiner, J.M. Lattimer, E.F. Brown, Astrophys. J. **722**, 33 (2010).
41. S. Guillot, M. Servillat, N.A. Webb, R.E. Rutledge, Astrophys. J. **772**, 7 (2013).
42. J.M. Lattimer, A.W. Steiner, Astrophys. J. **784**, 123 (2014).
43. C.O. Heinke *et al.*, Mon. Not. R. Acad. Sci. **444**, 443 (2014).
44. C.O. Heinke, J.E. Grindlay, D.A. Lloyd, P.D. Edmonds, Astrophys. J. **588**, 452 (2003).
45. F. Ozel, A. Gould, Tolga Guver, Astrophys. J. **748**, 5 (2012).
46. F. Ozel, D. Psaltis, T. Guver, G. Baym, C. Heinke, S. Guillot, arXiv:1505.05155v2.
47. W.C.G. Ho, C.O. Heinke, Nature **462**, 71 (2009).
48. C.O. Heinke, W.C.G. Ho, Astrophys. J. Lett. **719**, L167 (2010).
49. P.S. Shternin, D.G. Yakovlev, C.O. Heinke, W.C.G. Ho, D.J. Patnaude, Mon. Not. R. Acad. Sci. **412**, L108 (2011).
50. K.G. Elshamouty, C.O. Heinke, G.R. Sivakoff, W.C.G. Ho, P.S. Shternin, D.G. Yakovlev, D.J. Patnaude, L. David, Astrophys. J. **777**, 22 (2013).
51. B. Posselt, G.G. Pavlov, V. Suleimanov, O. Kargaltsev, Astrophys. J. **779**, 186 (2013).
52. W.C.G. Ho, K.G. Elshamouty, C.O. Heinke, A.Y. Potekhin, Phys. Rev. C **91**, 015806 (2015).
53. B. Posselt, G. Pavlov, V. Suleimanov, *Presentation at Workshop "The Many Faces of Neutron Stars", MIAPP Munich, Sept. 2015*, `http://www.munich-iapp.de/scientific-programme/programmes-2015/neutron-stars/schedule/`.
54. D. Page, M. Prakash, J.M. Lattimer, A.W. Steiner, Phys. Rev. Lett. **106**, 081101 (2011).

55. D. Blaschke, H. Grigorian, D.N. Voskresensky, F. Weber, Phys. Rev. C **85**, 022802(R) (2012).
56. A.Y. Potekhin, J.A. Pons, D. Page, Space Sci. Rev. **191**, 239 (2015).
57. H. Grigorian, D. N. Voskresensky, D. Blaschke, *Influence of the stiffness of the equation of state and in-medium effects on the cooling of compact stars*, contribution to this Topical Issue, arXiv:1603.02634.
58. T. Noda, M. Hashimoto, N. Yasutake, T. Maruyama, T. Tatsumi, M. Fujimoto, Astrophys. J. **765**, 1 (2013).
59. A. Sedrakian, Astron. Astrophys. **555**, L10 (2013).
60. A. Bonanno, M. Baldo, G.F. Burgio, V. Urpin, Astron. Astrophys. **561**, L5 (2014).
61. S.-H. Yang, C.-M. Pi, X.-P. Zheng, Astrophys. J. **735**, L29 (2011).
62. M.B. Tsang, J.R. Stone *et al.*, Phys. Rev. C **86**, 015803 (2012).
63. P. Danielewicz, Nucl. Phys. A **661**, 82 (1999)
64. P. Danielewicz, Nucl. Phys. A **673**, 375 (2000)
65. P. Danielewicz, Roy Lacey, W.G. Lynch., Science **298**, 1592 (2002).
66. Bao-An Li, Lie-Wen Chen, Che Ming Ko, Phys. Rep. **464**, 113 (2008).
67. C. Fuchs, Prog. Part. Nucl. Phys. **56**, 1 (2009).
68. W.G. Lynch, M.B. Tsang, Y. Zhang *et al.*, Prog. Part. Nucl. Phys. **62**, 427 (2009).
69. M.B. Tsang, Y. Zhang, P. Danielewicz *et al.*, Phys. Rev. Lett. **102**, 122701 (2009).
70. T. Furuta, A. Ono, Phys. Rev. C **79**, 014608 (2009).
71. R.H. Dalitz, A. Gal, Ann. Phys. **116**, 167 (1978).
72. B. Povh, Prog. Part. Nucl. Phys. **18**, 183 (1987).
73. Y. Yamamoto, T. Motoba, H. Himeno, K. Ikeda, S. Nagata, Prog. Theor. Phys. Suppl. **117**, 361 (1994).
74. A. Gal, Prog. Theor. Phys. Suppl. **156**, 1 (2004)
75. O. Hashimoto, H. Tamura, Prog. Part. Nucl. Phys. **57**, 564 (2006).
76. P.A.M. Guichon, A.W. Thomas, K. Tsushima, Nucl. Phys. A **814**, 66 (2008).
77. S. Bart *et al.*, Phys. Rev. Lett. **83**, 5238 (1999).
78. H. Noumi *et al.*, Phys. Rev. Lett. **89**, 072301 (2002) **90**, 049902(E) (2002).
79. P.K. Saha *et al.*, Phys. Rev. C **70**, 044613 (2004).
80. K. Nakazawa *et al.*, Prog. Theor. Exp. Phys. , 033D02 (2015).
81. M. Troyer, U.-J. Wiese, Phys. Rev. Lett. **94**, 170201 (2005).
82. G.P. Lepage, `http://arxiv.org/abs/hep-lat/0506036`.
83. R. Gupta, arXiv:hep-lat/9807028.
84. K. Fukushima, Y. Tanizaki, arXiv:1507.07351v1.
85. P.A.M. Guichon, Phys. Lett. B **200**, 235 (1988).
86. P.A.M. Guichon, A.W. Thomas, Phys. Rev. Lett. **93**, 132502 (2004).
87. D.L. Whittenbury, J.D. Carroll, A.W. Thomas, K. Tsushima, J.R. Stone, Phys. Rev. C **89**, 065801 (2014).
88. F. Bissey *et al.*, Phys. Rev. D **76**, 114512 (2007).
89. J.R. Stone, P.A.M. Guichon, H.H. Matevosyan, A.W. Thomas, Nucl. Phys. A **792**, 587 (2007).
90. P.A.M. Guichon, H.H. Matevosyan, N. Sandulescu, A.W. Thomas, Nucl. Phys. A **772**, 1 (2006).
91. P.A.M. Guichon, K. Saito, E.N. Rodionov, A.W. Thomas, Nucl. Phys. A **601**, 349 (1996).
92. K. Tsushima, K. Saito, A.W. Thomas, Phys. Lett. B **411**, 9 (1997).
93. K. Tsushima, K. Saito, A.W. Thomas, Phys. Lett. B **421**, 413 (1998).
94. J.R. Stone, N.J. Stone, S.A. Moszkowski, Phys. Rev. C **89**, 044316 (2014).
95. T. Miyatsu, T. Katayama, K. Saito, Phys. Letts. B **709**, 242 (2012).
96. T. Miyatsu, M.-K. Cheoun, K. Saito, Phys. Rev. C **88**, 015802 (2013).
97. T. Miyatsu, M.-K. Cheoun, K. Saito, JPS Conf. Proc. **1**, 013080 (2014).
98. J. Bartel, P. Quentin, M. Brack, C. Guet, H.-B. Hakansson, Nucl. Phys. A **386**, 79 (1982).
99. H.A. Bethe, M.B. Johnson, Nucl. Phys. A **230**, 1 (1974).
100. J. Schaffner-Bielich, Nucl. Phys. A **835**, 279 (2010).
101. J. Schaffner, I.N. Mishustin, Phys. Rev. C **53**, 416 (1996).
102. H.-J. Schulze, T. Rijken, Phys. Rev. C **84**, 035801 (2011).
103. I. Vidaa, D. Logoteta, C. Providncia, A. Polls, I. Bombaci, EPL **94**, 11002 (2011).
104. D. Lonardoni, F. Pederiva, S. Gandolfi, J. Phys.: Conf. Ser. **529**, 012012 (2014).
105. Y. Yamamoto, T. Furumoto, N. Yasutake, Th.A. Rijken, Phys. Rev. C **90**, 045805 (2014).
106. Y. Yamamoto, T. Furumoto, N. Yasutake, Th.A. Rijken, Eur. Phys. J. A **52**, 19 (2016) contribution to this Topical Issue.
107. A.V. Astashenok, S. Capozziello, S.D. Odintsov, Phys. Rev. D **89**, 103509 (2014).
108. B.D. Lackey, M. Nayyar, B.J. Owen, Phys. Rev. D **73**, 024021 (2006).
109. J.R. Stone, P.A.M. Guichon, P.-G. Reinhard, A.W. Thomas, Phys. Rev. Lett. **116**, 092501 (2016).
110. A.W. Thomas, P.A.M. Guichon, D.B. Leinweber, R.D. Young, Prog. Theor. Phys. Suppl. **156**, 124 (2004).
111. P. Klüpfel, P.-G. Reinhard, T.J. Bürvenich, J.A. Maruhn, Phys. Rev. C **79**, 034310 (2009).
112. P. Moller, J.R. Nix, W.D. Myers, W.J. Swiatecki, At. Data Nucl. Data Tables **59**, 185 (1995).
113. P.G. Reinhard, M. Bender, J.A. Maruhn, Comm. Mod. Phys. A **2**, 177 (2002).
114. `https://heasarc.gsfc.nasa.gov/docs/nicer/`.
115. A. Witze, Nature **511**, 2818 (2014).